

## Characteristics of large three-dimensional heaps of particles produced by ballistic deposition from extended sources

Nikola Topic<sup>a</sup>, Jason A.C. Gallas<sup>abc\*</sup> and Thorsten Pöschel<sup>ab</sup>

<sup>a</sup>*Institute for Multiscale Simulation, Friedrich-Alexander-Universität, D-91052 Erlangen, Germany;* <sup>b</sup>*Departamento de Física, Universidade Federal da Paraíba, 58051-970 João Pessoa, Brazil;* <sup>c</sup>*Instituto de Altos Estudos da Paraíba, Rua Infante Dom Henrique 100-1801, 58039-150 João Pessoa, Brazil*

(Received 9 January 2013; final version received 12 April 2013)

This paper reports a detailed numerical investigation of the geometrical and structural properties of three-dimensional heaps of particles. Our goal is the characterization of very large heaps produced by ballistic deposition from extended circular dropping areas. First, we provide an in-depth study of the formation of monodisperse heaps of particles. We find very large heaps to contain three new geometrical characteristics: they may display two external angles of repose, one internal angle of repose, and four distinct packing fraction (density) regions. Such features are found to be directly connected with the size of the dropping zone. We derive a differential equation describing the boundary of an unexpected triangular packing fraction zone formed under the dropping area. We investigate the impact that noise during the deposition has on the final heap structure. In addition, we perform two complementary experiments designed to test the robustness of the novel features found. The first experiment considers changes due to polydispersity. The second checks what happens when letting the extended dropping zone to become a point-like source of particles, the more common type of source.

**Keywords:** three-dimensional heaps of particles; ballistic deposition; heap formation; static sandpiles; granular matter

### 1. Introduction

A classical problem in the field of granular matter is the investigation of the peculiarities associated with both the genesis and the stability of heaps of particles. Heaps of particles are studied intensively because of their great relevance for industrial applications and because, from a theoretical point of view, such heaps are simple many-body systems well-suited to develop and probe theories [1,2]. The formation of grain heaps is important to understand theoretically and experimentally complex cooperative phenomena. One may easily list a series of complex granular phenomena that have attracted recurring interest over the years, e.g. studies addressing major effects like the characterization of the stress dip under the pile [3–12], avalanching behavior [13–16], segregation by size [17–19], creep motion deep in the pile [20] and the remarkable properties discovered in the growth of grain piles by revolving rivers [21–26], and many others [27–32].

---

\*Corresponding author. Email: [jason.gallas@cbi.uni-erlangen.de](mailto:jason.gallas@cbi.uni-erlangen.de)

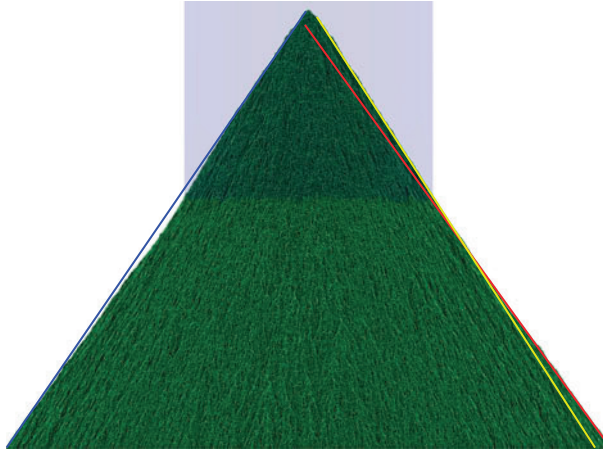


Figure 1. (colour online) Illustrative example of a typical heap obtained by dropping  $12 \times 10^6$  particles sequentially from the top of a circular area source with radius  $r = 80$  particles diameters. The three distinct tangent lines help to identify the presence of two angles of repose. Lines on the right side are tangent either to the top or to the bottom of the heap while the line on the left connects top and bottom of the heap.

The majority of studies presently available mainly explores properties of *two-dimensional* (2D) heaps of grains. For instance, a recent paper by Roul et al. [33] investigates packing properties of 2D piles of grains using sophisticated molecular dynamic simulations. Among other things, they reported the presence of a clear peak in the particle density around the middle of the heap arguing that local compactification and arching could perhaps explain such differences. Variations in the angle of repose of 2D heaps were investigated as a function of experimental parameters and deviations in the shape of the tail of 2D sandpiles were discovered [34]. Experiments and theory concerning the pressure dip under 2D grain piles along with some results for three-dimensional (3D) heaps were reported by Atman et al. [11] who find that the controversial presence or absence of pressure dips to be closely related to the preparation history of the pile, and call for more extensive systematic studies. The influence of the geometry on the pressure distribution of granular heaps was considered in an interesting work by Matuttis and Schinner [35].

The pile characteristics are basically determined by the forces that it experiences during the deposition process. Since lateral forces constraining 2D piles are quite different from the lateral forces acting in 3D piles, it seems natural to investigate systematically the structure of *three-dimensional* packings, which are subjected to more complex lateral forces, to see whether they contain hitherto unnoticed features. Despite the fact that static piles of granular materials are classical examples of packings, to date there has been no systematic study of spatially resolved packing properties of 3D heaps. By their own nature, three-dimensional heaps require the deposition of a large number of particles, of the order of two to three orders of magnitude more than those typically used in 2D scenarios.

The aim of the present paper is to report a study of the density distribution and the angle of repose measured for very large 3D heaps of particles. As an example of the unexpected results found, Figure 1 illustrates the existence of two angles of repose for a pile containing  $12 \times 10^6$  particles. We report results obtained for heaps with up to  $25 \times 10^6$  particles dropped sequentially onto a horizontal plane from a homogeneous “rain” of particles emerging from

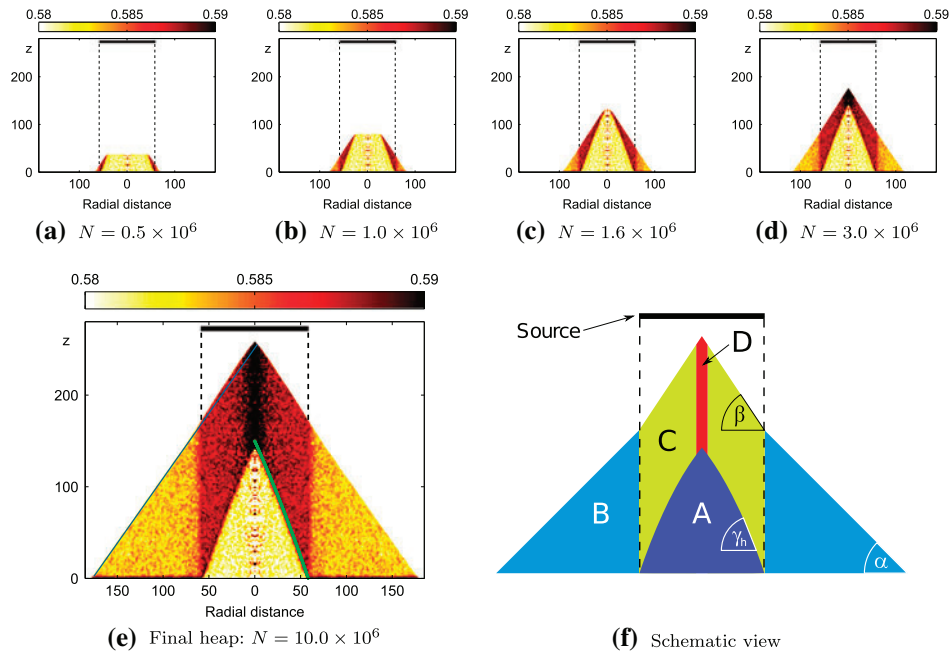


Figure 2. (colour online) Panels (a)–(d) illustrate the growth of a large three-dimensional heap obtained by dropping particles sequentially from the top of a circular area source with radius  $r = 60$  particle diameters. Note how the top flat horizontal surface shrinks as the growth proceeds. Panel (e) shows the final heap. The line segment on the right of the inner triangle shows the prediction obtained from Equation (9). The auxiliary straight line on the left heap boundary helps to visualize the existence of two external angles of repose. (f) Schematic representation summarizing the main geometric characteristics of large 3d heaps: the angles of repose  $\alpha$ ,  $\beta$ ,  $\gamma_h$ , where  $h$  is the elevation height at which the angle is measured, and the four axially symmetric density zones  $A$ ,  $B$ ,  $C$ ,  $D$ . The small curvature of the inner triangle  $A$  was enhanced for clarity. In all cases investigated the curvature can be well-approximated by a straight-line segment. All these characteristics depend on the size (radius) of the rain of particles, indicated by the word “source”.

a circular area-source with adjustable radius. Our main aim is to determine bulk properties such as density, contact numbers, repose angles, etc. Simulations of large three-dimensional heaps are hardly feasible with a full molecular dynamics approach. However, there are efficient alternative ways to investigate a number of effects for such heaps. For example, simpler models normally used to describe ballistic deposition and related surface growth problems can provide useful insight for specific problems as the ones considered here.

In this work we adopt the well-known Visscher–Bolsterli (VB) algorithm [14,19,36–38] to investigate structural properties of very large three-dimensional heaps of particles. The VB algorithm was employed in pioneering work by Jullien and Meakin [19] to study size segregation in 3D heaps containing some  $4 - 40 \times 10^3$  particles. As mentioned, here we consider very large 3D heaps involving typically  $10 - 25 \times 10^6$  particles, i.e. about  $10^3$  more particles. In the VB algorithm, the particles are dropped one by one onto a growing deposit (see Figure 2). Particles follow the path of steepest descent until they stop after reaching either a local stable minimum or when touching the ground. After stopping, particles are not allowed to move anymore so that many-particle effects like, e.g. avalanches, cannot

be simulated although a plethora of other effects are nicely reproduced [14,19,37,38]. The VB algorithm is realistic for sandpiles grown under certain well defined conditions: When each particle follows the steepest descent path, that is, when effects of inertia are negligible. This may be achieved experimentally by sedimenting particles in an (almost density matched) viscous fluid. Alternatively, weakly adhesive particles would also perform a creeping motion. The key advantage of the sequential VB algorithm is that it provides a realistic framework to rapidly compute the path of steepest descent and, therefore, allows us to investigate very large assemblies of particles, not accessible with other models. We now describe our main findings.

The paper is organized as follows. In the first part (Sections 2–7) we study monodisperse heaps. In Section 2, we provide details of the deposition process and report the main findings for monodisperse heaps. We report three new geometrical characteristics, namely, that large heaps may have (i) two external angles of repose, (ii) an internal angle of repose, and (iii) four distinct packing fraction (density) regions. Section 3 describes a simple numerical experiment that we did in order to find out how noise affects the deposition process. In Section 4, we investigated the contact number distribution. In Section 5, we derive a differential equation whose solution provides a relation between the two new angles of repose as a function of the height  $h$  of the heap. For reference, in Section 6 we analyze two special cases of heaps: two-dimensional heaps, which can only display a single angle of repose, and three-dimensional heaps with small number of particles. In Section 7, we describe the characteristic of large heaps formed by deposition from a point, not from an extended source. A preliminary report about some results concerning monodisperse heaps was presented in Ref. [39]. In Section 8, we investigate the impact of polydispersivity on the structure of large heaps. Finally, Section 9 summarizes our main observations and mentions briefly some interesting open problems.

## 2. Packing densities and two angles of repose in monodisperse heaps

Panels (a)–(d) of Figure 2 show the growth-history of the packing fraction as a function of the radial distance from the heap axis for a 3D heap made of  $N = 10 \times 10^6$  particles when deposited sequentially from random positions in the extended circular source area whose diametral section is indicated by the solid black bar. In this and in subsequent figures, all sizes are measured in adimensional units  $r/d$ , where  $d$  is the (arbitrary) diameter of the particles. From panels (a)–(d) one sees how the inner triangular density cone gets formed when the top flat horizontal surface gets smaller and smaller as the particle deposition proceeds. The packing fraction displayed by the colors was obtained using cylindrical coordinates  $(r, z, \phi)$  coaxial with the heap. For masses  $m_i$  with center of mass at  $\mathbf{r}_i$  we measured the density  $\rho(r, z, \phi)$  at  $\mathbf{r}$  using the definition [40]

$$\rho(\mathbf{r}) \equiv \sum_i m_i \varphi(\mathbf{r} - \mathbf{r}_i), \quad (1)$$

where  $\varphi(\mathbf{r})$  is a Gaussian coarse-graining function

$$\varphi(\mathbf{r}) = \frac{1}{\pi^{3/2} w^3} e^{-(|\mathbf{r}|/w)^2}, \quad w = 2R, \quad (2)$$

and  $R$  is the particle radius. Then, by averaging  $\rho(r, z, \phi)$  over  $\phi$  we get the density distribution  $\bar{\rho}(r, z)$ , the quantity that is color-coded in Figure 2.

An interesting question is to understand how the packing fraction varies along large heaps produced by deposition from extended area sources. This may be recognized both from distribution of colors of the final heap depicted in Figure 2(e) and from the summarizing sketch presented in Figure 2(f). Generically, we could distinguish up to four rather distinct density (packing) regions: First, under the dropping zone we find a triangular region indicated by the letter *A*. The lateral surface of this cone are slightly curved, as described by a differential equation, Equation (9), below. Second, as area *A* grows more and more, particles may eventually roll outside the circular “shadow” of the dropping area (source), forming another packing zone that we denote by *B*. Since the VB algorithm requires particles to roll maintaining always contact with the heap, in region *B* the particles are arranged more regularly than in *A*, where the heap must grow on top of a randomly deposited initial layer, not on a the more regular layer arising from “rolling” (i.e. not from random deposition). Third, comes region *C* where we find an intermediary packing that is less regular than in *B* but more regular than in *A*. Finally, near the axis of the heap over region *A* we find zone *D* characterized by the highest density of the heap.

For the heap shown in Figure 2, containing  $N = 10 \times 10^6$  particles, we computed the following densities well-inside each region:  $\rho_A = 0.5812 \pm 0.0002$ ,  $\rho_B = 0.5832 \pm 0.0002$ ,  $\rho_C = 0.5879 \pm 0.0002$ , and  $0.59 \pm 0.02 < \rho_D < 0.63 \pm 0.02$ . The relative values of these densities is the same found for other heaps. If we approximate the boundaries between regions by straight lines, then the corresponding angles of repose are found to be  $\alpha = (54.5 \pm 0.5)^\circ$ ,  $\beta = (57.5 \pm 0.5)^\circ$ , and  $\gamma = (68 \pm 0.4)^\circ$ , measured directly from the final heap (Figure 2(e)). The origin of the differences in density are the distinct sedimentation mechanism at work in each region.

The distinct density zones described above have some remarkable implications for the geometrical characteristics of the heap, specially for the angle of repose. The most striking implication is that, instead of the familiar single angle of repose, we find large three-dimensional heaps to display a conspicuous *pair of external angles of repose*, in addition to an *internal angle of repose* formed by the boundary between *A* and *C* in Figure 2(f). As may be recognized with the help of the auxiliary straight line on the left side of the heap in Figure 2(e), under the dropping area one finds a larger angle of repose than outside it. There are two distinct limits of interest here. When the dropping zone shrinks, region *B* overtakes *C* (and *A*). In contrast, the contrary happens if the noise during the deposition increases, with *C* overtaking *B*. The “familiar” angle of repose is the final single angle that results after taking anyone of these limits.

The pair of external angles was measured as follows. For every  $z_i$ , we located the set of points  $r_i$  defining the outermost surface points around the heap, plotting them as  $r = r(z)$ . Then, using bins with  $\Delta r = 10$  particle diameters, we fitted a straight line through the points  $(r_i, z_i)$  for each bin obtaining the dependence of the local angle of repose  $\theta$  as a function of the distance  $r$  from the axis.

Figure 3 shows the evolution of the angle  $\theta$  of repose as a function of the distance  $r$  from the axis of the heap. From this figure it is easy to recognize the characteristic discontinuities found in the external angle of repose as well as the magnitudes of the angles inside and outside the rain of particles. Error bars represent deviations recorded when sampling over five distinct heaps and show that the variations of the angles are much larger than the fluctuations resulting from sampling different heaps. The existence of two angles of repose can be observed qualitatively already with a simple “kitchen table” experiment [39].

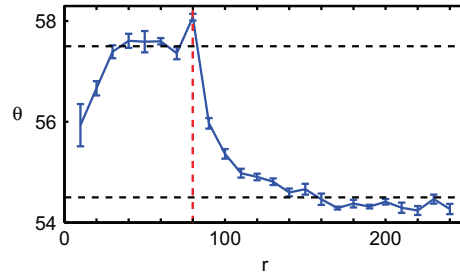


Figure 3. (colour online) Evolution of the angle  $\theta$  of repose as a function of the distance  $r$  from the axis. Note the clear discontinuity at  $r = 80$ , the vertical dashed line, indicating the radius of the dropping zone. The angle of repose is larger under the rain of particles. The heap underlying the determination of  $\theta$  here contains  $N = 25 \times 10^6$  particles;  $r$  is measured in units of particle diameters.

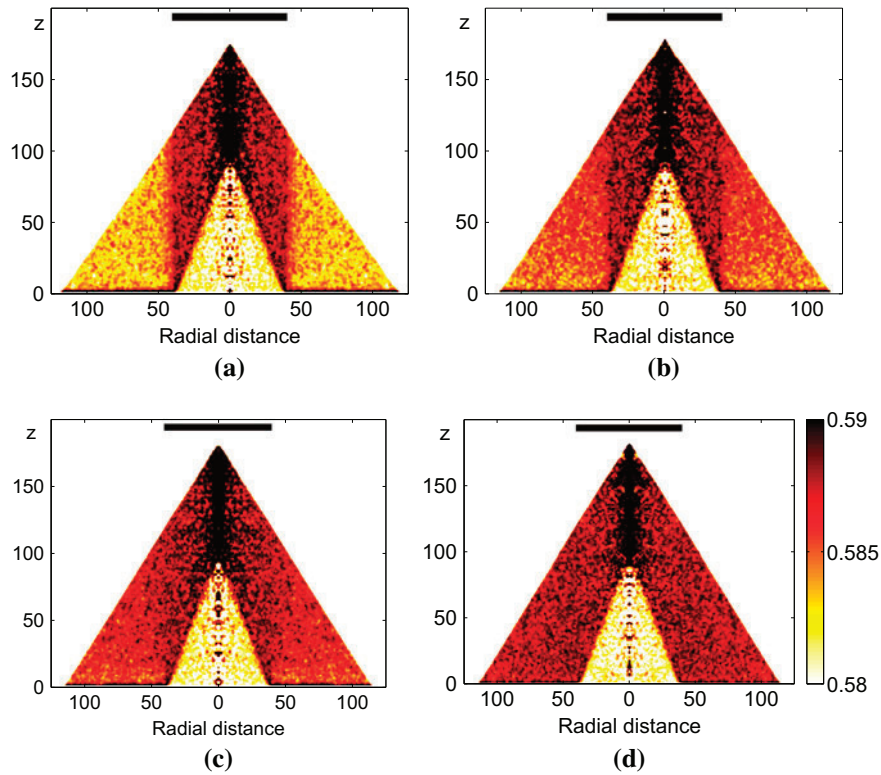


Figure 4. (colour online) Effect of noise in the deposition process. The plots show density fields. In the leftmost panel the heap was never perturbed ( $e = \infty$ ). The other three panels, from left to right, show heaps formed when applying with an increasing frequency a random perturbation, namely after every 512, 128 and 32 “events” (see text) corresponding, approximately, to particles traveling downwards for about 160, 40, and 10 particle diameters, respectively. Region  $B$  is overtaken by  $C$  as random noise during the deposition increases. Each panel displays  $N = 3 \times 10^6$  particles.

### 3. Effect of noise in the deposition process

While sequential deposition means that particles follow strictly the path of steepest descent, noise of any origin may occasionally interrupt such path by relocating the particle to a random position in a close neighborhood of its original position, thereby allowing previously unaccessible minima to suddenly become accessible. Therefore, it becomes desirable to understand how angles of repose and density zones are affected by random fluctuations like, e.g. saltation of grains, which are necessarily present during experimental deposition processes.

To have an idea of the impact of noise during the deposition we performed a simple numerical experiment which consisted of perturbing periodically the down-hill rolling movement after the particle had a certain number  $e$  of “events” in the pile, i.e. after it had the opportunity of falling long enough so as to have changed its contacts  $e$  times on its way down. Thus, after falling down unperturbed during  $e$  events, the particle was then lifted vertically from its position  $(x, y)$  and dropped randomly at a nearby location  $(x + \Delta x, y + \Delta y)$ , where  $\Delta x$  and  $\Delta y$  are random numbers such that  $(\Delta x)^2 + (\Delta y)^2 < 9R^2$ , where  $R$  is the radius of the particles.

Figure 4 illustrates the result of such experiment for increasing noise strength: one clearly sees that regions  $B$  and  $C$  become “mixed”, i.e. indistinguishable, as the perturbation frequency increases (from left to right). Since the correlation of the deposition process is destroyed by noise, Figure 4 indicates that strong noise during deposition is responsible for the increasingly higher density observed in the  $B$  zone (when compared with the density in  $C$ ). Remarkably, zones  $A$  and  $D$  remain essentially unaffected by noise. A clear result of this experiment is to show that deposition strongly affected by noise may prevent the possibility of observing the external pair of angles of repose.

### 4. Contact number distribution of monodisperse heaps

A classical measure to characterize the packing structure of spheres is to compute the average number of contacts among particles [41]. Accordingly, we determined the average number of contacts in a similar way as described above for the density after replacing  $\rho(\mathbf{r})$  by  $c(\mathbf{r}) = (\sum_i c_i)/n$ , where  $c_i$  and  $\mathbf{r}_i$  are the number of contacts and position of particle  $i$ , and  $n$  is the total number of particles inside of the averaging volume. Figure 5 shows the result of such counting. It is clearly consistent with our findings described above, in particular with the geometrical picture summarized in Figure 2(f).

The average contact number in Figure 5 shows two interesting novel features: a pronounced jump in contact number as one crosses the boundary from  $A$  to  $C$ , and a dip between  $C$  and  $B$ . The boundary between  $A$  and  $C$  corresponds to a “transition zone” where the top flat surface observed in the earlier stages of the construction of the heap disappears or where the tilted surface meets the flat surface. This sharp transition zone corresponds to an area of high contact number where the surface curvature is high (see Figure 2(e)). Accordingly, we assume the local surface curvature to be responsible for the changes in the average contact numbers. The local curvature can be determined from the surface  $r(z)$  described above. This assumption is of course consistent with the peak in contact numbers near the axis (area  $D$ ): close to the top of the heap the mean curvature becomes very high.

The dip in contact number between areas  $B$  and  $C$  corresponds to points where the angle of repose changes from  $\alpha$  to  $\beta$ . Change in the angle of repose causes lower or even

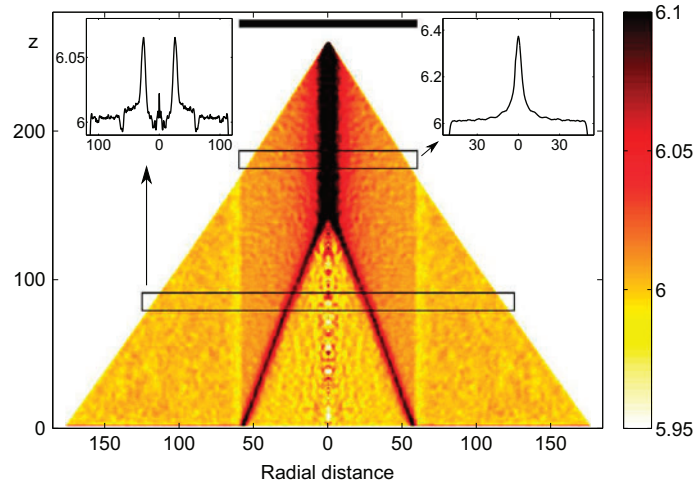


Figure 5. (colour online) Typical profiles of the average contact number inside of the heap shown as a function from radial distance from the heap axis. The pair of rectangles indicated the region used to compute the variation of contact number (see text). Here  $N = 10^7$ .

negative mean curvatures, a fact consistent with the drop in the number of contacts. We explain this as a simple geometrical effect. Recall that a particle stopping on a flat surface will have three contact in addition to the contacts from the particles deposited on top of it. If a particle is deposited onto a surface having a positive mean curvature (e.g. an sphere), it will have three contact from the particle below it but, thanks to the curved surface, there is more space for contacts from particles deposited on top of it, leading to an increase in the number of contacts. For negative curvature the reverse happens: there is less space for new contacts, causing a decrease in contact number.

### 5. Relation between the two new angles of repose in monodisperse heaps

As it is clear from Figure 2(f), the angles  $\alpha$ ,  $\beta$ , and  $\gamma$  are not independent from each other. Therefore, we now derive a relation interconnecting them. During the initial phase of the growth the heap has a top flat surface (see panels (a)–(d) in Figure 2). Particles falling on this flat surface stay on it, since it is only a quite negligible amount falls of the edge. Particles that fall onto the tilted surface form a layer of approximately constant thickness on the whole inclined surface of the heap. From these assumptions and, for simplicity, working with an “average” angle  $\delta = (\alpha + \beta)/2$ , it is not difficult to derive a differential equation for  $r(h)$ , the function describing how the radius  $r$  of the flat surface shrinks as a function of the height  $h$  of the heap.

Let the quantities  $r$ ,  $S$ ,  $h$ ,  $\delta$  define the geometry of the heap as illustrated in Figure 6. We wish to find a relation between the angle of repose  $\delta$  and the change in the area  $dr/dh$  of the top flat surface of the heap under the simplifying assumptions that the heap has constant density, a single angle of repose, that it grows symmetrically, and that the material added to lateral surface has constant thickness. From Figure 6 it follows that  $s = x \sin(\gamma - \delta)$  and

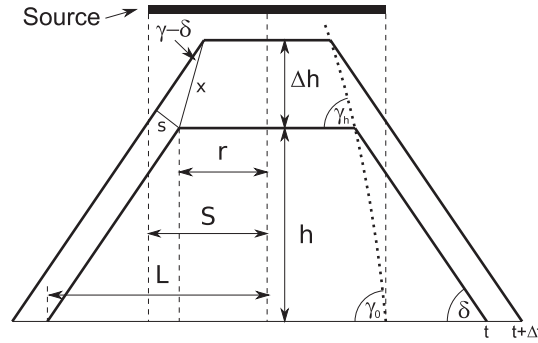


Figure 6. Schematic view of a central section of the symmetrically growing heap, characterized by the  $h$ -dependent angle  $\gamma \equiv \gamma_h$ , drawn for times  $t$  and  $t + \Delta t$  (ticker lines). The random “rain” of particles originates from a circular source with radius  $S$ . For clarity, the distance between the source and the heap was greatly reduced here.

$\Delta h = x \sin \gamma$  so that, eliminating  $x$ , we get:

$$\frac{s}{\Delta h} = \frac{\sin(\gamma - \delta)}{\sin \gamma}. \quad (3)$$

This relation may be obtained in another way, as follows. The assumption of constant density implies that  $V = V_t + V_f$ , where  $V$  denotes the total volume of deposited material at time  $\Delta t$ ,  $V_t$  the volume deposited on the *tilted* surface, and  $V_f$  is the volume on the *flat* surface. When  $\Delta t$  is small, the volume contained between flat and tilted surface becomes negligible and the particles being deposited end up located either on the flat surface of radius  $r < S$  or inside the lateral tilted surface. Since particles are dropped as a homogeneous rain through the area source, the number of particles that fall onto the flat surface of the heap in time  $\Delta t$  is  $N_f = \pi r^2 F \Delta t$ . Here  $F$  is the particle flux through the source, i.e. the number of particles that pass through the unit area of the source in unit time. Since the total number of particles passing through the whole source in an interval  $\Delta t$  is  $N = \pi S^2 F \Delta t$ , we find that the number of particles that end up on the tilted surface is  $N_t = N - N_f = \pi(S^2 - r^2) F \Delta t$ .

For constant packing fraction  $n$ , the number of particles  $N_f$  that fall onto the flat surface contributes to the change of  $\Delta h$ ,

$$\pi r^2 F \Delta t = n \pi r^2 \Delta h \quad (4)$$

and  $N_t$  contributes to  $s$ ,

$$\pi(S^2 - r^2) F \Delta t = n s \pi \frac{L^2 - r^2}{\cos \delta}, \quad (5)$$

where  $\pi(L^2 - r^2)/\cos \delta$  is the surface of the frustum.

From Equations (4) and (5) we obtain

$$\frac{s}{\Delta h} = \frac{S^2 - r^2}{L^2 - r^2} \cos \delta. \quad (6)$$

Comparing Equations (3) and (6) one readily sees that

$$\frac{\sin(\gamma - \delta)}{\sin \gamma} = \frac{S^2 - r^2}{L^2 - r^2} \cos \delta \quad (7)$$

Now, using the addition formula for the sin function and the relation  $L = r + h \cot \delta$  extracted from the figure, we obtain:

$$\tan \gamma = \frac{(r + h \cot \delta)^2 - r^2}{(r + h \cot \delta)^2 - S^2} \tan \delta. \quad (8)$$

Thus, since  $dr/dh = -\cot \gamma$ , we obtain a differential equation for  $r(h)$ , the function describing how the flat surface shrinks in time:

$$\frac{dr}{dh} = -\cot \gamma = -\frac{(r + h \cot \delta)^2 - S^2}{(r + h \cot \delta)^2 - r^2} \cot \delta. \quad (9)$$

The proper initial condition is  $r(h = 0) = S$ . The negative sign indicates that the area shrinks from its initial value.

Of course, this equation is only physically meaningful as long as  $r \geq 0$ . The solution obtained by numerical integration for  $S = 60$  is shown by the straight line in Figure 2(e). Solving the equation for  $h = 0$  we get  $\gamma_0 \equiv \gamma(h = 0) = \arctan(2 \tan \delta) = 71^\circ$ . Note that Equation (9) can be rescaled with respect to  $S$  in such a way that only  $r/S$  and  $h/S$  appear in it. This means that Equation (9) is scale invariant and needs to be solved just once, thanks to the relation  $r_S(h) = x r_{S/x} \left( \frac{h}{x} \right)$ .

## 6. Two-dimensional heaps and small systems

Is it possible to find two angles of repose in two-dimensional heaps? In two dimensions, the packing outside the dropping zone degenerates into a (trivial) hexagonal packing for the following reason: Each particle which reaches the floor outside the dropping zone must be in contact with another particle (on which it rolled down). Therefore, outside the dropping zone the particles on the floor form a connected line of identical spheres. The next layer will sediment in the local minima between the particles in the first layer and, consequently, also touch one another. Iterating this procedure, a hexagonal packing of particles emerges. Therefore, the packing in two dimensions will have a very different (trivial) structure as compared to the three-dimensional case.

To illustrate more clearly what happens under VB ballistic deposition in two dimensions, Figure 7 presents three snapshots taken during the growth of a heap. In the initial phase, shown in Figure 7(a), the impact of the random layer deposited directly under the dropping zone is quite large since the random layer generates dislocations that propagate towards the boundaries, producing rather rough lateral surfaces. Here, growth occurs by steepest-descent on complex dislocation hillocks, and involves the formation and incorporation of small, mobile little clusters arising from the initial randomly deposited bead layer. Defects in the form of hollow channels are observed and persist indefinitely during the growth. Although such dislocations remain always present, Figure 7(b) shows that the relative impact of the dislocations on the lateral surfaces is greatly reduced as the deposition proceeds. From this figure is also not difficult to recognize that the heap consists mainly of three large domains of hexagonal packings which are separated by the persistent dislocation lines. In the limit of large number of particles (as shown in Figure 7(d)) only a single asymptotic angle of repose is visible, with the bump produced by the dislocation lines (magnified in Figure 7(c)) becoming less and less distinguishable. Figure 7(e) illustrates how the lateral surface grows as more and more particles are added to the heap. Thus, large two-dimensional heaps reveal just a hexagonal packing and its characteristic angle of repose of  $60^\circ$ .

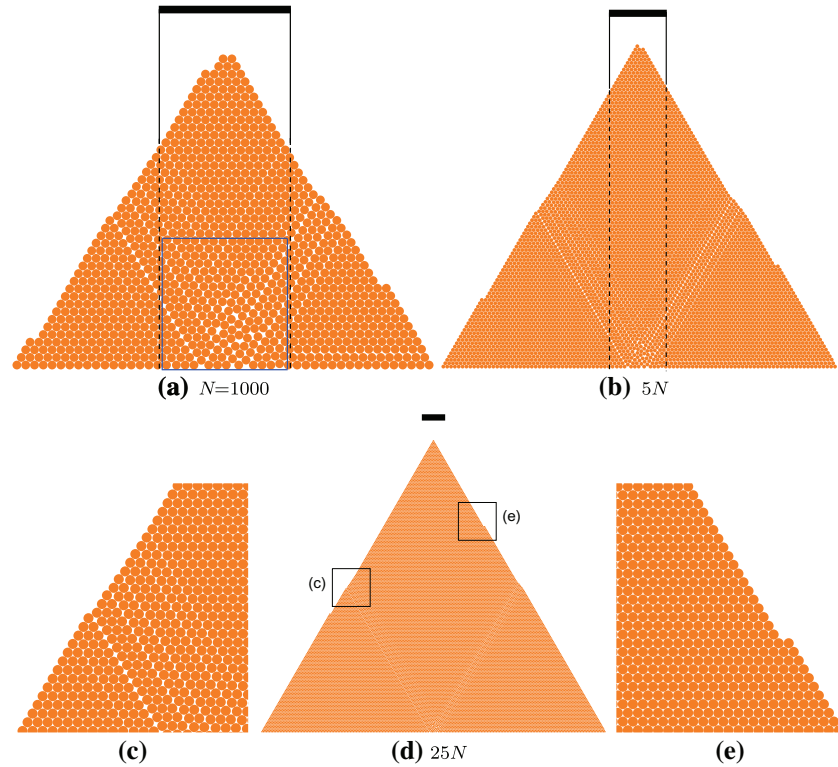


Figure 7. (colour online) Three consecutive snapshots of a growing two-dimensional heap of particles sedimented from a line source (indicated as a black bar) of length 15 particle diameters. The rectangle in (a) contains the area from which the dislocation lines originate (c) shows the dislocations on the left surface while in (e) one sees the characteristic hexagonal packing (see text). Note: scales are not the same for these snapshots. The size of the black bar provides a reference. The lateral growth occurs by steepest-descent on complex dislocation hillocks, and involves the formation and incorporation of small, mobile little clusters arising from the initial randomly deposited bead layer. Defects in the form of hollow channels are observed and persist indefinitely during the growth.

Why are large systems necessary to identify the two angles of repose and the four density regions? The effect of different densities in regions A–D is a small (but reproducible) effect. In numbers, the difference in density between regions B and C is a small fraction of a percent (see color scale in Figure 2). The difference between A and B is yet smaller. To generate the density plots in the  $(r, z)$ -plane shown in Figures 2, 4, 8 from the full 3-dim representation  $(r, z, \phi)$  and the corresponding fields of coordination number in the  $(r, z)$ -plane shown in Figures 5, 8, we average (integrate, sum) over the angle  $\phi$ . Only with this averaging we obtain smooth enough fields to reliably distinguish the different regions A–D. If the heap would be small, the average over  $\phi$  would correspond to only few particles located in a certain interval  $(r + \Delta r, z + \Delta z)$ , in particular for small values of  $r$ . Consequently, in order to obtain significant results for the density in the  $(r, z)$ -plane, allowing to distinguish sub-percent differences, we need a large enough heap. Alternatively, we could also simulate many smaller heaps to obtain the fields at the same low noise level, however, the total number of sedimented particles (either on one heap or on many heaps) would be invariant.

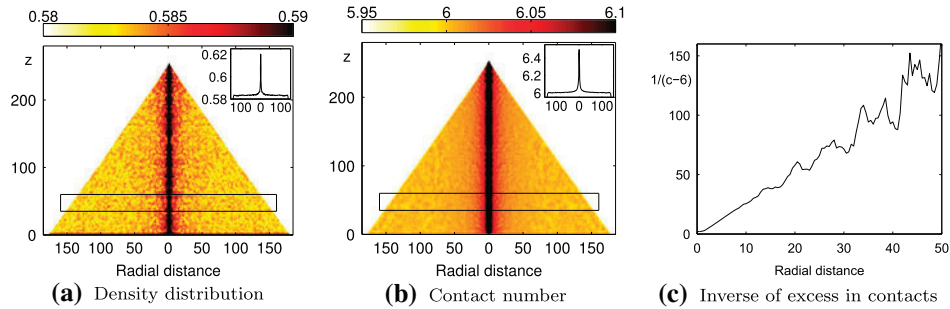


Figure 8. (colour online) (a) Distribution of density inside of the heap created from a point source. The inset shows the density averaged in  $z$  direction inside of the black rectangle. (b) Distribution of contact number. The inset shows the changes in contact number,  $c$ , obtained by the same averaging as in (a). The fields represent an average over five different heaps, each one containing  $N = 10^7$  particles. (c) Inverse of excesses of contact number as a function of the distance from the axis, calculated from the contact number from the inset of (b).

## 7. Point source density and contact number of monodisperse heaps

For comparison purposes, we now consider monodisperse heaps, obtained when particles are deposited from a fixed point (not from extended sources as before). Point sources are interesting because they appear often in industrial settings and in experiments dealing with, for example, the stress distribution under the pile [3–9, 11, 12]. Obviously, since point source is a limiting case of area source, it can be used as an additional check of the geometrical picture given in Figure 2. We look at the density fields, the contact number and the angles of repose.

We start by considering the distribution of density and contact number. Particles with same radius,  $R = 1/2$ , are dropped from a fixed point high above the heap onto the flat horizontal plane. If a particle lands exactly on top of another one it is allowed to roll in a random direction. The density distribution inside the heap is shown in Figure 8(a). Particles are most tightly packed in the region around the heap axis. Further away from the axis the packing fraction quickly approaches a constant value. The point source can be obtained from an area source if we let the radius of the dropping zone tend to zero, and therefore two highest density zones  $C$  and  $D$  will merge, forming a single zone after matching at the axis of the heap. The area  $A$  will disappear, leaving only two zones: a zone of high density near the axis and lower density everywhere else. This prediction matches very well the measured density distribution, Figure 8(a). The distribution of contact number shows the same trend as the density, as may be seen from Figure 8(b).

What is the functional relationship between the average contact number,  $c$ , and the distance  $r$  from the axis? To obtain  $c$  at some  $r$ , we average the field,  $\bar{c}(r, z)$ , in the  $z$  direction for a certain section of the heap, indicated by a black rectangle in Figure 8(b). There is approximately a linear dependence between  $1/(c - 6)$  and the distance from the axis, Figure 8(c), implying that  $c - 6 \sim 1/r$ . The quantity  $c - 6$  is the excess of contact number as compared to average for the VB packings. Since the surface of the heap is approximately conical and, therefore, its mean surface curvature decays as  $\sim 1/r$ , there is a linear relationship between the excess of contact number,  $c - 6$ , and mean surface curvature.

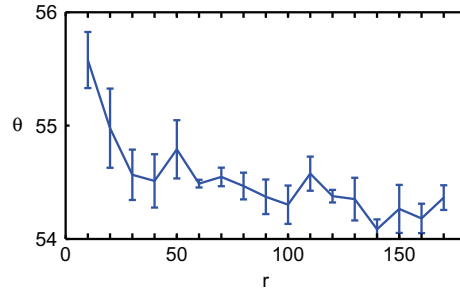


Figure 9. (colour online) Angle of repose  $\theta \equiv \theta(r)$  computed for a monodisperse heap deposited from a point source. For each  $r$  the angle of repose represents an average obtained over five heaps, each one containing  $N = 10^7$  particles. The errors are standard errors of the mean value of  $\theta$  measured at fixed distance from the axis for five independent heaps.

How does the angle of repose varies with the distance from the axis for a heap deposited from a point source? This is shown in Figure 9. For a heap with  $N = 10^7$  particles and base radius of  $L = 180$  particle diameters our numerical experiments show that the change in the angle of repose for  $r > 30$  is less than  $0.25^\circ$ , while in the vicinity of the axis  $r < 30$  the total change is around  $\Delta\theta = 1^\circ$ . The magnitude of such changes are close to the estimated statistical errors. Therefore, the heap has a shape close to a cone, particularly away from the axis. This is at variance with the results for the heap created from an extended area source, where an angle variation of  $\simeq 3^\circ$  can appear at any distance from the axis, depending on the size of the area source.

### 8. Effect of polydispersity on the heap structure

Strongly polydisperse particles are of importance in industrial applications [43], while at the same time realistic granular particles are never precisely monodisperse. Therefore, it is of interest to understand the effect of polydispersity on the structure of the heap and compare it with the monodisperse limit. Packings produced with particles having power-law distribution of radii have been shown by numerical and analytical tools to have high packing fractions when compared to other distributions [44–46]. Due to this special status, we choose a power-law distribution of particle radii, namely  $f(R) = A/R^3$ , where  $R$  is particle radius, with  $f(R)dR$  being the probability of having a particle in the range  $(R, R + dR)$ . In this type of distribution, to each interval  $dR$  of radii corresponds a constant volume  $dV = \frac{4}{3} \frac{A}{R^3} R^3 \pi dR = \frac{4}{3} A \pi dR$  and, therefore, each species of particle radius contributes equally to the total volume contained in the particles. Denoting minimal and maximal particle radii by  $R_{\min}$  and  $R_{\max}$ , from the normalization condition  $1 = A \int_{R_{\min}}^{R_{\max}} dR \frac{1}{R^3}$ , it follows that  $A = 2R_{\min}^2 R_{\max}^2 / (R_{\max}^2 - R_{\min}^2)$ .

As a working *measure of polydispersity* we use the ratio between the maximal and minimal radius,  $\alpha = R_{\max}/R_{\min}$ . For a fair comparison among heaps, we require that two heaps having the same number of particles have the same mass. From this condition it follows that  $\langle R^3 \rangle = \text{constant}$ . For the monodisperse case,  $\alpha = 1$ , we have  $\langle R^3 \rangle = 1/8$ , under the assumption that we deal with monodisperse particles having radius  $R = 1/2$ .

Now we need to calculate  $R_{\min}$  and  $R_{\max}$  in order to fix the distribution of polydisperse particles. From  $\langle R^3 \rangle = 1/8$  and our measure of polydispersity it follows that

$$R_{\min} = \sqrt[3]{\frac{1 + \alpha}{16\alpha^2}}, \quad \text{and} \quad R_{\max} = \alpha R_{\min}. \quad (10)$$

As it is known, the packing fraction is the basic indicator of the packing structure of the heap, and we now wish to examine how its distribution is modified as compared to the monodisperse heap created from an area source. In particular we are interested in how the geometrical picture of density distribution, from Figure 2(f) is affected. For the computation of the density of the polydisperse heap we again use Equation (1). The width of the coarse graining function,  $w$ , is taken to be  $w = 2\sqrt[3]{\langle R^3 \rangle} = 1$ , where the average is done over a set of particle radii from one heap. As before, to obtain the final density distribution we perform the averaging around the axis of the heap.

For heaps with polydispersity  $\alpha = 3$  and  $N = 25 \times 10^6$  particles we find that the total density, Figure 10(a), is higher than for the monodisperse heap, Figure 10(b). More significantly, in the polydisperse heap the density observed in the area  $A$ ,  $\rho_A = 0.6051 \pm 0.0002$ , is no longer the lowest one, but area  $B$  now has the lowest density,  $0.593 < \rho_B < 0.598$  (statistical error is much smaller than the variations across the area  $B$ ). The characteristic densities of areas  $A$  and  $C$ ,  $0.6032 \pm 0.0003 < \rho_C < 0.6052 \pm 0.0004$ , may have now nearly equal values. In summary, areas  $A$ ,  $B$  and  $C$  have higher densities when compared to the monodisperse heap, but for polydisperse heaps it is area  $A$  which has the highest increase, matching the density of area  $C$ . The slower increase of the density in areas  $B$  and  $C$  as compared to area  $A$  indicates that, on a tilted surface, pores between bigger particles are less efficiently filled with small particles than on a flat surface. Less efficient filling of pores can be caused by segregation on the tilted surface, and segregation is known to appear in polydisperse heaps created with VB algorithm [19]. In addition, there is a jump in density near the boundary of areas  $A$  and  $C$ . Such jump is non-existent or too weak to be noticeable for monodisperse heaps. This jump appears at the same position as the jump observed in contact numbers for monodisperse heaps, namely, at the boundary between areas  $A$  and  $C$ .

We now consider the effect of polydispersity on the average contact numbers inside of the heap. For the contact number we used the same counting procedure as for the monodisperse system. The distribution of contact number for a heap with  $\alpha = 3$  is shown in Figure 10(c) and, as a comparison, also for the monodisperse heap, Figure 10(d). Polydispersity does not influence the partition of the heap into four zones of contact number, neither the dip in contact number at the boundary between area  $B$  and  $C$  nor the jump at  $A$ – $C$  boundary. In other words, the four zones reported here seem to be quite robust. For the polydisperse heap the contact number distribution in area  $B$  is more inhomogeneous than in the monodisperse heap, and we can observe two distinctive features: (i) The average contact number are higher near the ground in the layer of thickness  $10 - 20$ , (ii) The existence of thin stripes parallel to the heap surface.

For the polydisperse heap we can look at how the average particle radii changes throughout the heap. To calculate the distribution of average radii we sort the particles by their  $z$  coordinate and distance from the axis  $r$  of the heap into a two dimensional lattice with vertices  $(r_i, z_j)$ , where a particle with coordinates  $(r, z)$  is sorted into the  $(i, j)$  cell if  $r_i < r < r_{i+1}$  and  $z_j < z < z_{j+1}$ . We then sum the radii of all particles belonging to each

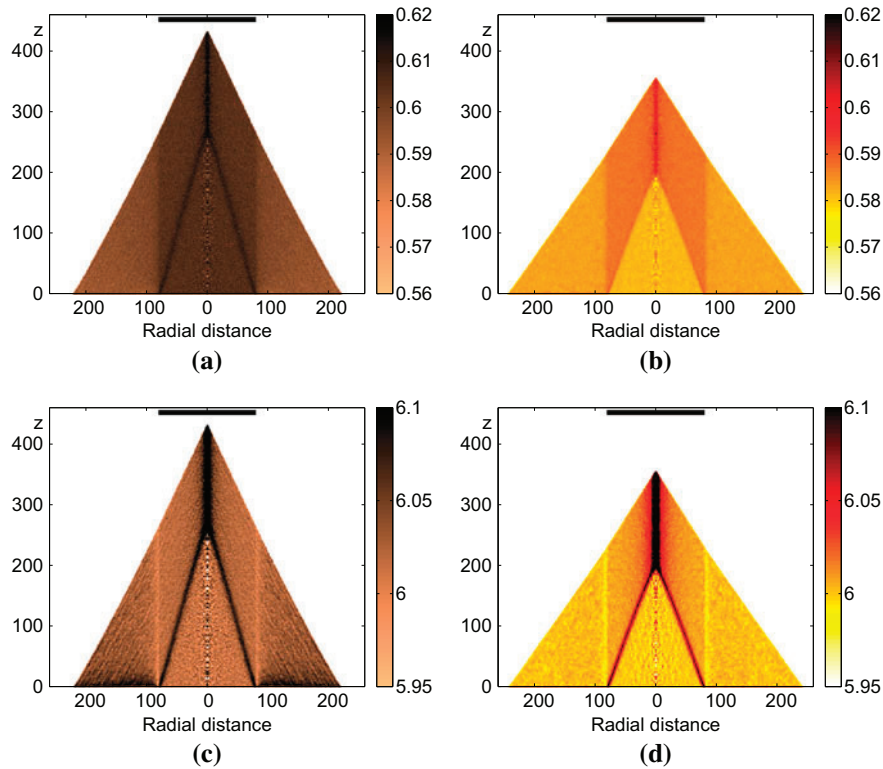


Figure 10. (colour online) Comparison of the packing properties between a polydisperse heap with  $\alpha = R_{max}/R_{min} = 3$  (left column) and a monodisperse heap,  $\alpha = 1$ , (right column). Panels (a) and (b) [top row] compare the density distribution inside of the heap, while panels (c) and (d) [bottom row] compare the distribution of contact number. The areas  $A$ ,  $B$ ,  $C$  and  $D$  still exist in the polydisperse heap. Additionally, a jump in density appears between areas  $A$  and  $C$ . The average packing density is considerably higher for polydisperse heaps. Notable inhomogeneities appear in the area  $B$  for  $\alpha = 3$ . All fields are average over five heaps, each containing  $N = 25 \times 10^6$  particles.

cell and divide such sum by the total number of particles in this cell to obtain the average radius for this cell. The result of this measurement for heaps with polydispersities  $\alpha = 1.2$ ,  $\alpha = 1.5$ ,  $\alpha = 2$  and  $\alpha = 3$  is shown in Figure 11. From this figure we see that the heap can be separated into three sections with sharp boundaries, and they correspond to density zones  $A$ ,  $B$  and  $C$ . It is possible to recognize that smaller particles “prefer” to go inside of area  $C$ . Area  $B$  is inhomogeneous, with the largest particles located near the bottom.

We conclude this Section illustrating in Figure 12 how the angle of repose changes in heaps of polydisperse particles. Such angles are calculated using the same procedure used to calculate such angle in the monodisperse heap. We look at the same heaps that were used to compute the distribution of average radii inside the heap. Our simulations show that polydispersity produces a sharp increase in the angle of repose. Analogously as for monodisperse heaps, there is a change in the angle of repose as the boundary of the dropping zone is crossed, but this change is much weaker for stronger polydispersity. However, in contrast with monodisperse heaps, for polydisperse heaps the angle of repose outside the rain of particles does not tend to a constant value (Figure 12) and, therefore,

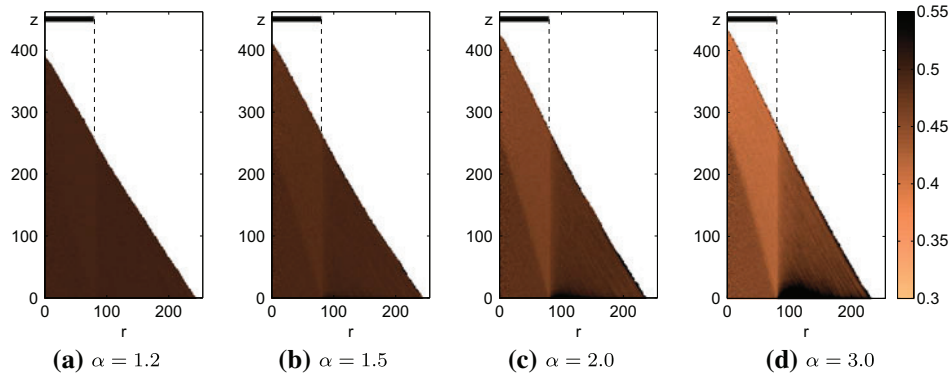


Figure 11. (colour online) Distribution of average particle radii inside polydisperse heaps created by dropping particles with radii distribution  $f(R) \sim 1/R^3$  from an extended area source, indicated by the black rectangle on the top. Polydispersity increases from left to right. The colormap corresponds to average particle radius at some  $(r, z)$  inside of the heap, (see text). As for monodisperse particles, there is a clear correspondence between zones A, B, C and D (compare with Figure 2(f)). Smaller particles have a preference for area C. Large particles accumulate near the bottom of area B. Striations due to segregation may be seen for higher values of  $\alpha$  (see text).

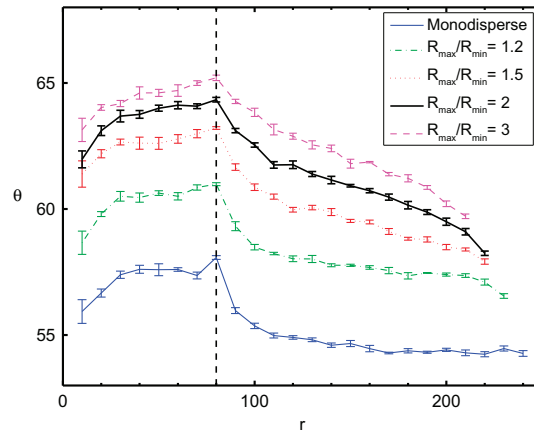


Figure 12. (colour online) Effect of the polydispersity on the angle of repose  $\theta$  for particles dropped from an area source extending up to  $r = 80$ . Polydispersity grows from the bottom trace to the top. Outside the rain  $\theta$  gets clearly washed out as polydispersity grows. Each data set represents an average over five distinct heaps made of  $N = 25 \times 10^6$  particles, while the error bars are standard errors of the mean value of  $\theta$  measured at fixed distance from the axis.

polydisperse heaps do not show two angles of repose, but only one, locate inside of the dropping zone.

### 9. Conclusions and outlook

Our numerical analysis of large three-dimensional heaps revealed a number of unexpected and remarkable features. As summarized in Figure 2(f), the novel geometrical properties

are as follows: (i) two external angles of repose  $\alpha$  and  $\beta$ , (ii) an internal angle of repose  $\gamma$ , and (iii) four distinct density (packing fraction) regions,  $A$ ,  $B$ ,  $C$ ,  $D$ . In other words, instead of just the familiar single angle of repose [42], heaps may in fact show two distinct angles, a fact that implies the existence of four distinct density zones in the heap. Such properties can be recognized both in the density distribution and in the distribution of the number of contacts. We showed the external and internal angles of repose,  $\alpha$  and  $\gamma$ , to be interrelated according to Equation (9), a relation involving explicitly the radius  $S$  of the dropping zone (“rain” of particles). We conducted a series of experiments to assess the impact of noise on the final heap. Such experiments indicated that the duality of the angle of repose may be washed out by moderate to strong noise during the deposition process. We have also simulated ballistic deposition in two dimensions and shown that in this simpler case there is only a single angle of repose underlying the characteristic hexagonal packing of this configuration.

Finally, an important aspect described here concerns how polydispersity affects the several characteristic features reported here. As described in details in Section 8, our simulations indicate that polydispersity alters more significantly both the magnitude and the density distribution of the heap. We expect the several new effects described to be easier to observe in rains where grains do not interact (low density rain) and when suppressing or minimizing the action of inertia, e.g. by performing experiments in an ambient of a viscous fluid, or building heaps using adhesive particles. Once a particle gets in touch with an already sedimented particle, it still can slowly roll under the action of gravity, but it would not exert any inertial forces. We hope that our present work will trigger more research in this direction, both experimentally and theoretically. Possible theoretical directions involve study of other rain geometries and introduction of more realistic models of deposition.

### Acknowledgements

The authors thank the Deutsche Forschungsgemeinschaft (DFG) for funding through the Cluster of Excellence Engineering of Advanced Materials and within the frame of the Collaborative Research Initiative “Additive Manufacturing” (SFB 814). JACG is also supported by CNPq, Brazil.

### References

- [1] B. Cambou, M. Jean and F. Radjai (eds.), *Micromechanics of Granular Materials*, Wiley, New York, 2009.
- [2] T. Pöschel and N. Brilliantov (eds.), *Granular Gas Dynamics*, Springer, Berlin, 2010.
- [3] F.H. Hummel and E.J. Finnan, Proc. Inst. Civil Eng. 212 (1921) p.369.
- [4] T. Jotaki and R. Moriyama, J. Soc. Powder Technol. Japan 60 (1979) p.184.
- [5] J. Smid and J. Novosad, *Pressure Distribution Under Heaped Bulk Solids*, Powtech Conf. Ind. Chem. Eng. Symp. 63 (1981) D3/V/1.
- [6] R. Brockbank, J.M. Huntley and R.C. Ball, J. Phys. II(7) (1997) p.1521.
- [7] L. Vanel, D. Howell, D. Clark, R.P. Behringer and E. Clement, Phys. Rev. E 60 (1999) p.R5040.
- [8] S. Luding, Phys. Rev. E 55 (1997) p.4720.
- [9] L. Vanel, P. Claudin, J.P. Bouchaud, M.E. Cates, E. Clement and J.P. Wittmer, Phys. Rev. Lett. 84 (2000) p.1439.
- [10] K. Littman, M. Nguyen, G. Metcalfe and P. Cleary, Gran. Matter 3 (2001) p.165.
- [11] A.P.F. Atman, P. Brunet, J. Geng, G. Reydellet, P. Claudin, R.P. Behringer and E. Clement, Eur. Phys. J. E 17 (2005) p.93.

- [12] J.Y. Ooi, J. Ai, Z. Zhong, J.F. Cheng and J.M. Rotter, *Progressive pressure measurements beneath a granular pile with and without base deflection*, in *Structures and Granular Solids: From Scientific Principles to Engineering Application*, J.G. Teng, J.Y. Ooi and J.F. Chen, eds., Taylor & Francis, London, 2008, p. 87.
- [13] A. Daerr and S. Douady, *Nature* 399 (1999) p.241.
- [14] A. Higgins, *J. Phys. A* 29 (1996) p.2373.
- [15] G.A. Held, D.H. Solina, D.T. Keane, W.J. Haag, P.M. Horn and G. Grinstein, *Phys. Rev. Lett.* 65 (1990) p.1120.
- [16] H.M. Jaeger, C.H. Liu and S.R. Nagel, *Phys. Rev. Lett.* 62 (1989) p.40.
- [17] M. Shimokawa and S. Ohta, *Phys. Rev. E* 77 (2008) p.011305.
- [18] H.A. Makse, S. Havlin, P.R. King and H.E. Stanley, *Nature* 386 (1997) p.379.
- [19] R. Jullien and P. Meakin, *Nature* 344 (1990) p.425.
- [20] T.S. Komatsu, S. Inagaki, N. Nakagawa and S. Nasuno, *Phys. Rev. Lett.* 86 (2001) p.1757.
- [21] E. Altshuler, O. Ramos, E. Martínez, A.J. Batista-Leyva, A. Rivera and K.E. Bassler, *Phys. Rev. Lett.* 91 (2003) p.014501.
- [22] E. Altshuler, R. Toussaint, E. Martínez, O. Sotolongo-Costa, J. Schmittbuhl and K.J. Måløy, *Phys. Rev. E* 77 (2008) p.031305.
- [23] T. Shinbrot, *Eur. Phys. J. E* 22 (2007) p.209.
- [24] T. Shinbrot, N.-H. Duong, M. Hettenbach and L. Kwan, *Gran. Matter* 9 (2007) p.295.
- [25] X.-Z. Kong, M.-B. Hu and Q.-S. Wu, *Phys. Lett. A* 348 (2006) p.77.
- [26] C. Urabe, *J. Phys. Soc. Japan* 74 (2005) p.2475.
- [27] C.F.M. Magalhães, J.G. Moreira and A.P.F. Atman, *Eur. Phys. J. E* 35 (2012) p.38.
- [28] M. Heckel, P. Müller, T. Pöschel and J.A.C. Gallas, *Phys. Rev. E* 86 (2012) p.061310.
- [29] T. Pöschel, D. Rosenkranz and J.A.C. Gallas, *Phys. Rev. E* 85 (2012) p.031307.
- [30] J.A.C. Gallas, H.J. Herrmann, T. Pöschel and S. Sokołowski, *J. Stat. Phys.* 82 (1996) p.443.
- [31] T. Pöschel and H.J. Herrmann, *Europhys. Lett.* 29 (1995) p.123.
- [32] J.A.C. Gallas, H.J. Herrmann and S. Sokołowski, *Phys. Rev. Lett.* 69 (1992) p.1371.
- [33] P. Roul and A. Schinner, *Powder Technol.* 204 (2010) p.113.
- [34] Y. Grasselli and H.J. Herrmann, *Eur. Phys. J. B* 10 (1999) p.673.
- [35] H.G. Matuttis and A. Schinner, *Gran. Matter* 1 (1999) p.195.
- [36] W.M. Visscher and M. Bolsterli, *Nature* 239 (1972) p.504.
- [37] R. Jullien and P. Meakin, *Coll. Surf. A* 165 (2000) p.405.
- [38] R. Jullien, A. Pavlovitch and P. Meakin, *J. Phys. A* 25 (1992) p.4103.
- [39] N. Topic, J.A.C. Gallas and T. Pöschel, *Phys. Rev. Lett.* 109 (2012) p.128001.
- [40] I. Goldhirsch and C. Goldberg, *Eur. Phys. J. E* 9 (2002) p.245.
- [41] J.D. Bernal and J. Mason, *Nature* 188 (1960) p. 910. See also Refs. [1,2].
- [42] H. Maleki, F. Ebrahimi and E.N. Oskoe, *J. Stat. Mech.* 2008 (2008) p.P04026.
- [43] E. Masoero, E. Del Gado, R.J.M. Pellenq, F.J. Ulm and S. Yip, *Phys. Rev. Lett.* 109 (2012) p.155503.
- [44] C. Voivret, F. Radjai, J.-Y. Delenne and M.S. El Youssoufi, *Phys. Rev. E* 76 (2007) p.021301.
- [45] T. Aste, *Phys. Rev. E* 53 (1996) p.2571.
- [46] H.J.H. Brouwers, *Phys. Rev. E* 74 (2006) p.031309.